Available online at www.sciencedirect.com
SCIENCE DIRECT
Journal of Solid State Chemistry 179 (2006) 2562–2570
JOURNAL OF SOLID STATE CHEMISTRY
www.elsevier.com/locate/jssc

Fabrication and photoelectrochemical properties of porous $ZnWO_4$ film

Xu Zhao, Wenqing Yao, Yan Wu, Shicheng Zhang, Haipeng Yang, Yongfa Zhu*

Department of Chemistry, Tsinghua University, Beijing 100084, PR China

Received 16 February 2006; received in revised form 29 April 2006; accepted 7 May 2006
Available online 13 May 2006

Abstract

Porous $ZnWO_4$ films have been fabricated on Indium–tin oxide (ITO) glass and its photoelectrochemical properties and high photocatalytic activities towards degradation of rhodamine B (RhB) has been investigated. Using amorphous heteronuclear complex as precursor and with the addition of polyethylene glycol (PEG, molecular weight = 400), the porous $ZnWO_4$ films have been achieved at the temperature of 500 °C via dip-coating method. It is composed of approximately 70 nm-sized particles and exhibits substantial porosity. The textures and porosity of $ZnWO_4$ films are dependent on preparation factors, such as the ratio of precursor/PEG and the annealing conditions. The formation mechanism of porous $ZnWO_4$ films was proposed. The porous $ZnWO_4$ films exhibited high photocatalytic activities towards degrading RhB. The top of valence band and the bottom of the conduction band was estimated to be −0.56 and 3.45 eV (vs. saturated calomel electrode (SCE)), respectively.

Keywords: $ZnWO_4$ film; Photoelectrochemistry; Photocatalysis

1. Introduction

Semiconductor photocatalysts have attracted much interest due to their potential applicability in detoxification of environmental pollutants [1] and solar energy conversion [2] recently. In addition to traditional photocatalysts such as TiO_2, WO_3, CdS, and Ta_2O_5 [3,4], many vanadate, niobates, and tantalates have exhibited excellent photocatalytic activities recently [5–7]. Thus, the transitional metal complex oxides have attracted much attention.

Many tungstates had excellent electro-optic behaviors owing to its good intrinsic physical and chemical properties. Bi_2WO_6 [8,9] and $AgInW_2O_8$ [10] have exhibited high photocatalytic activities. However, there are still little reports on the photocatalytic performances and phtoelectrochemical properties of tungstates. $ZnWO_4$ belongs to the monoclinic group of tungstates. It has been widely studied due to its intriguing luminescence behavior, structure, properties, and potential applications such as optical fibers, scintillator materials, magnetic properties, and heterogeneous catalysis [11–15]. However, its photocatalytic activities and photoelectrochemical properties has not been revealed.

Porous semiconductor films with high surface-area have attracted much attention due to the applications in electronic, photoelectrochemical, and photocatalytic systems [2,16]. Spanhel et al. prepared the $ZnWO_4$ film via the colloidal synthesis of $ZnO–WO_3$ heteroaggregates [17]. This method presented the possibility to produce transparent blue fluorescing $ZnWO_4$ coatings unavailable by conventional fabrication. However, the $ZnWO_4$ crystalline was aggregated upon the annealing process. Cocivera fabricated $ZnWO_4$ thin films on glass substrate by spray pyrolysis [12]. This method is inconvenient and the grain size of the resultant $ZnWO_4$ was large. The complex metal oxide film or powder materials with nanosized structure can be prepared from heteronuclear complex [18–20]. However, preparation of porous $ZnWO_4$ films via this method has not been reported yet.

Herein, the porous $ZnWO_4$ film was fabricated from amorphous heteronuclear complex via the addition of polyethylene glycol (PEG), which induces the formation of the porous structures during the annealing process. The film exhibited excellent photocurrent response and high photocatalytic activities towards the degradation of

*Corresponding author. Fax: +86 10 62787601.
E-mail address: zhuyf@mail.tsinghua.edu.cn (Y. Zhu).

0022-4596/$ - see front matter © 2006 Elsevier Inc. All rights reserved.
doi:10.1016/j.jssc.2006.05.004

rhodamine B (RhB) under UV light irradiation. Its photoelectrochemical properties were explored.

2. Experimental section

2.1. Fabrication of the $ZnWO_4$ film

Indium–tin oxide (ITO) glass was purchased from China Southern Class Co. Ltd., with a thickness of 1.1 mm and a sheet resistance of 15 Ω/□. All other chemicals were analytical grade reagents and used without further purification. Deionized water was used throughout the experiment. Porous $ZnWO_4$ films on ITO glass were prepared from an amorphous heteronuclear complex via the dip-coating method. All other chemicals were analytical grade reagents and used without further purification. Given amounts of $5(NH_4)_2O \cdot 12WO_3 \cdot 5H_2O$ were dissolved in deionized water and then were mixed with certain amounts of $Zn(NO_3)_2 \cdot 6H_2O$. Following, given amounts of citric acid was added into above suspension as a chelating agent for the metal ions. The molar ratio of metal ions to citric acid was 1:2. The solution was stirred for 2 h. A precursor was obtained by drying the above solution at 80 °C for 3 days. The precursor is mainly consisted of Zn, W, N, O and H elements. Using the dip-coating method, the precursor dissolved in aqueous solution with a certain amount of PEG was deposited onto an ITO glass, and fired at various temperatures in air for given time. In comparison, TiO_2 film was prepared via Sol–Gel process by dip-coating method. The TiO_2 sol was prepared as follows: A 20-mL aliquot $Ti(OC_4H_9)_4$ (AR) was added dropwise at room temperature to 160 mL ethanol (AR) and then 3 mL of $NH(C_2H_4OH)_2$ was added to the solution. After stirring with an ultrasonic horn for 15 min, a light-yellow transparent solution was formed. After gelatinized for 48 h, the precursor solution was mixed with 160 mL 98% (V/V) ethanol solution. Sealed and gelized for 72 h, a sol with TiO_2 concentration of 16 g/L was obtained. The above procedure has been given in our previous article [21]. The obtained TiO_2 film is not porous and with a thickness of ca. 85 nm.

2.2. Characterization of the $ZnWO_4$ film

The morphology of the $ZnWO_4$ film was characterized by a JSM 6301 electron-scanning microscope (SEM). Raman spectra were used to estimate the crystal phase. Fourier-transform infrared (FT-IR) spectroscopy is used to provide some information for the $ZnWO_4$ film formation, which was conducted on a Renishaw RM1000 spectroscope. The wavelength of the laser light was 514 nm. X-ray diffraction (XRD) was performed on the X-ray Diffractometer (Japan, Rigaku, D/max-RB). TG and DTA analyses were performed on a Du Pont Universal V2.6D thermal analyzer. The atmosphere was air and the heating rate was 10 °C/min. FT-IR spectroscopy (Spectrum GX, Perkin-Elmer Company) is used to provide some information for the $ZnWO_4$ film formation. A JEOL JEM-1200EX transmission electron microscope (TEM) with the accelerating voltage of the electron beam of 120 kV was used to observe the size of $ZnWO_4$ particles, which are scratched off the film samples. High-resolution transmission electron microscopy (HRTEM) images were obtained by JEM 2010F field emission gun TEM operated at an accelerating voltage of 200 kV. The Auger electron spectroscopy (AES) technique was used to determine the thickness of the film. The energy and beam current of the Ar ion beam were 3.0 keV and 6 μA, respectively. The beam diameter was 1 mm and the sputtering rate was approximately 30.0 nm/min. X-ray photoelectron analysis was measured on a PHI 5300 ECSA instrument using an Al Ka X-ray source at a power of 250 W. The binding energy scale was calibrated with respect to the C1s photopeak of hydrocarbon contamination fixed at 285.0 eV.

2.3. Photoelectrochemical experiments

For photoelectrochemical measurement, a Cu wire was attached to the $ZnWO_4$ film with ITO substrate with epoxy resin to prevent current leakage. A quartz electrolytic cell was employed, filled with 100 mL of 0.5 M Na_2SO_4 solution. A Pt wire and a saturated calomel electrode (SCE) were employed as the counter and reference electrodes, respectively. A 20 W germicidal lamp (~90% of energy output at 253.7 nm) was used as irradiation source. The intensity of light, as measured by an UV-irradiance meter (UV-A, Instruments of Beijing Normal University) was 19 $\mu W/cm^2$ at 4 cm into the reactor, the position where the $ZnWO_4$ film electrode was placed. The photoelectrochemical experiment was carried out with a computerized CHI660B electrochemical system (Shanghai, China). Photocatalytic degradation of RhB was performed with the initial concentration of 5 mg/L in 100 mL 0.5 M Na_2SO_4 solution. Its concentrations were examined using Hitachi U-3010 UV-Vis spectrophotometer.

3. Results and discussion

3.1. Texture and structure of the porous $ZnWO_4$ film

The precursor film was obtained by drying the precursor solution with the initial concentration of 22% and the addition of PEG (6 wt%) at 80 °C for 4 h. As shown in Fig. 1, it was uniform and its morphologies change with the annealing temperature. The samples heated at 450 °C consist of a network of ca. 120 nm long round particles, which is assigned to the precursor complex. At 500 °C, the $ZnWO_4$ films are formed, which is homogeneous and composed of about 70 nm sized, regular particles and exhibits substantial porosity. At 550 °C, the particle size of $ZnWO_4$ and pores become large and the porous structures is relatively clear. Further, the $ZnWO_4$ particles were scratched off the film samples treated at 500 and 550 °C and analyzed by the TEM, respectively. As illustrated in

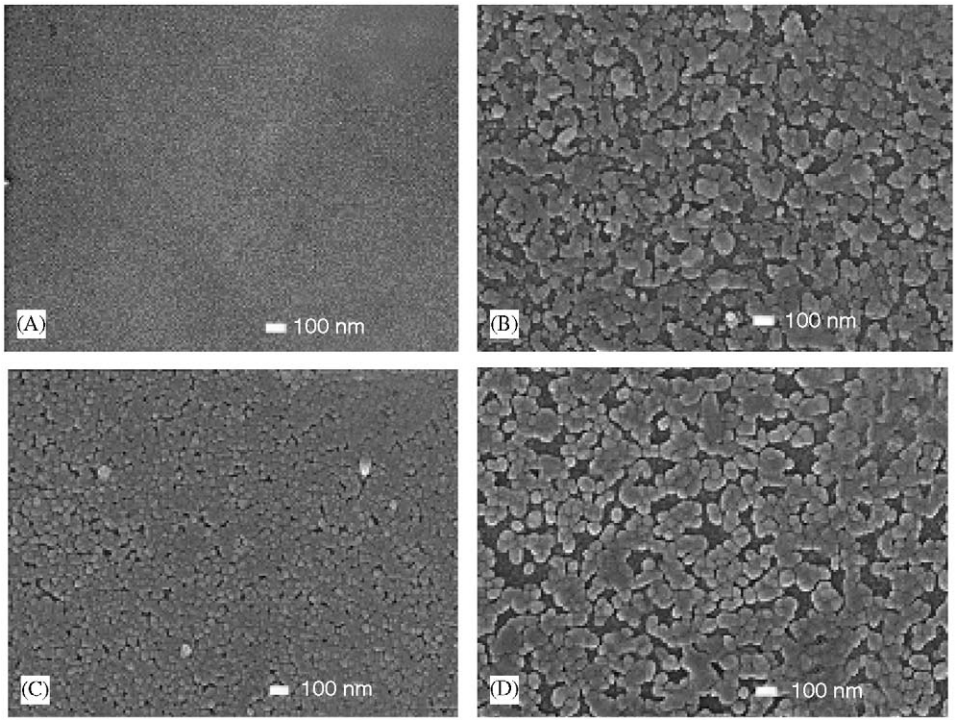

Fig. 1. SEM micrographs of the precursor film (A) and calcined at 450 °C (B), 500 °C (C), and 550 °C (D).

Fig. 2, the particles sizes for the samples treated at 500 and 550 °C are ca. 70 and 150 nm, respectively. Furthermore, no different appearances were observed in the HRTEM of the $ZnWO_4$ sample scratched from the $ZnWO_4$ film and $ZnWO_4$ powder sample obtained at 500 °C for 4 h. It is clear that the $ZnWO_4$ powder is not porous. These results confirm the results that the porosity of the $ZnWO_4$ is induced by the particle aggregation.

The influence of PEG concentration on the surface texture of $ZnWO_4$ film is investigated. Without the addition of the PEG, large particles were observed (Fig. 3(A)). With the addition of 4% PEG, the films become homogeneous, small particles were observed, and uniform pores appear (Fig. 3(B)). The PEG suppresses the agglomeration of the $ZnWO_4$ particles and induces the formation of pore structures during the calcination process. However, when the PEG concentration is increased to 8% and 10%, the sizes of particles and pores become large (Fig. 3(C) and (D)). And, the number of $ZnWO_4$ particles on the surface of the film decrease. With the increase in PEG concentration the production of gas amount increase during the calcination process, which enlarge the pore diameter and particle sizes and decrease the number of $ZnWO_4$ particles. No cracks are found in the $ZnWO_4$ film, which lead to its high mechanical stability.

Fig. 4(A) shows the Raman patterns for the precursor film treated at various temperatures for 4 h. At 450 °C, the precursor film was amorphous. The $ZnWO_4$ crystals appear at 500 and 550 °C. The $ZnWO_4$ crystals were seen more clearly for the film sample which was deposited for three times, where the deposition of the precursor and calcinations was repeated for three times. XRD patterns of the film treated at 500 °C for three times, $ZnWO_4$ powder, and ITO substrate are shown in Fig. 4(B). The appearance of peaks at 15°, 19, 31°, 41°, and 45° for the film samples confirm the formation of monoclinic wolframite structure of $ZnWO_4$ phase. Furthermore, the XPS analysis of the $ZnWO_4$ film surface calcined at 500 °C for 4 h was performed; the result shown in Fig. 5 further confirmed the formation of $ZnWO_4$ film.

The effect of calcination time on the crystallization of $ZnWO_4$ was investigated at the constant temperature of 500 °C. The results (Fig. 6) indicated that the $ZnWO_4$ phase was formed within 1 h. The peak intensity increase when the calcinations time is extended to 2 h. Further increase in the calcination time plays little effect on the crystal phase of $ZnWO_4$. As shown in Fig. 7, the AES depth profile spectra of the $ZnWO_4$ film samples coated for three times indicated that the thickness of the $ZnWO_4$ film was ca. 75 nm. The thickness of film samples coated for one time was ca. 25 nm. In addition, it also did not show evidence of interdiffusion or chemical reaction at the film/ITO substrate interface.

3.2. Formation process of the porous $ZnWO_4$ film

In order to explore the formation process of the porous $ZnWO_4$ film, the decomposition process of the precursor powders was first investigated using TG and DTA spectra. As shown in Fig. 8, with the increase of temperature, the weight loss occurs in the TG curve up to 550 °C. Thereafter, the weight remains constant, indicating that the

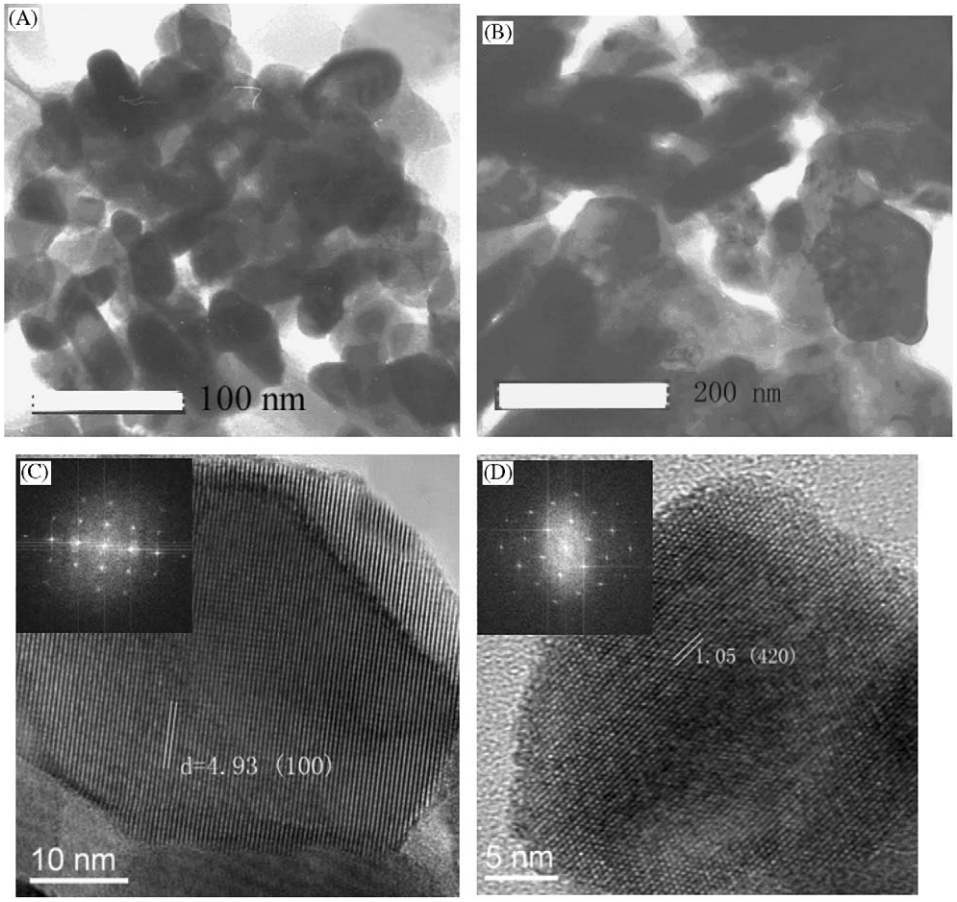

Fig. 2. TEM of $ZnWO_4$ particles scratched off the films calcined at 500 °C (A) and 550 °C (B). HRTEM analysis of the $ZnWO_4$ sample scratched from the film (C) and the $ZnWO_4$ powder sample (D).

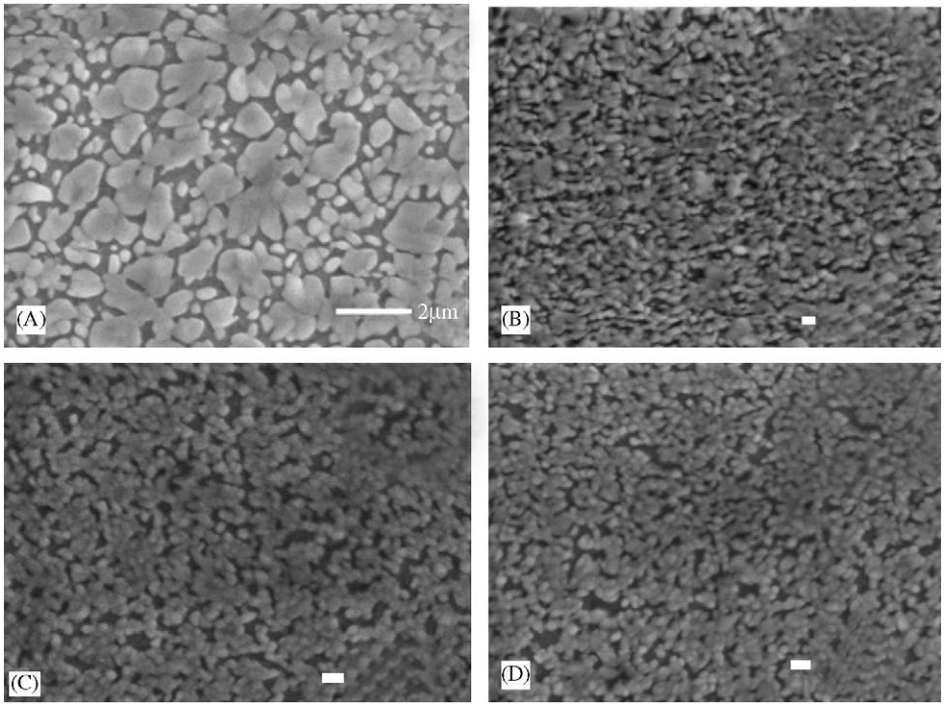

Fig. 3. SEM micrographs of the $ZnWO_4$ films deposited onto ITO glass plate calcined at 500 °C for 4 h. without PEG (A) and with various content of PEG ((B) 4%; (C) 8%; and (D) 10%) in the precursor solution with the concentration of 20%.

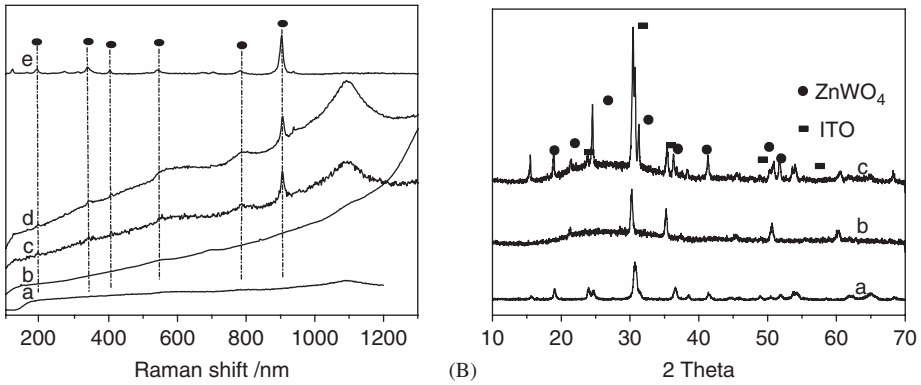

Fig. 4. (A) Raman spectra of $ZnWO_4$-coated ITO plate with different calcined temperature: (a) ITO substrate; (b) $ZnWO_4$-25 nm-450 °C; (c) $ZnWO_4$-25 nm-500 °C; (d) $ZnWO_4$-25 nm-550 °C; and (e) $ZnWO_4$-75 nm-500 °C. (B) XRD patterns of $ZnWO_4$ powder (a), ITO plate (b), and $ZnWO_4$-coated ITO plate (c) treated at 500 °C (75 nm).

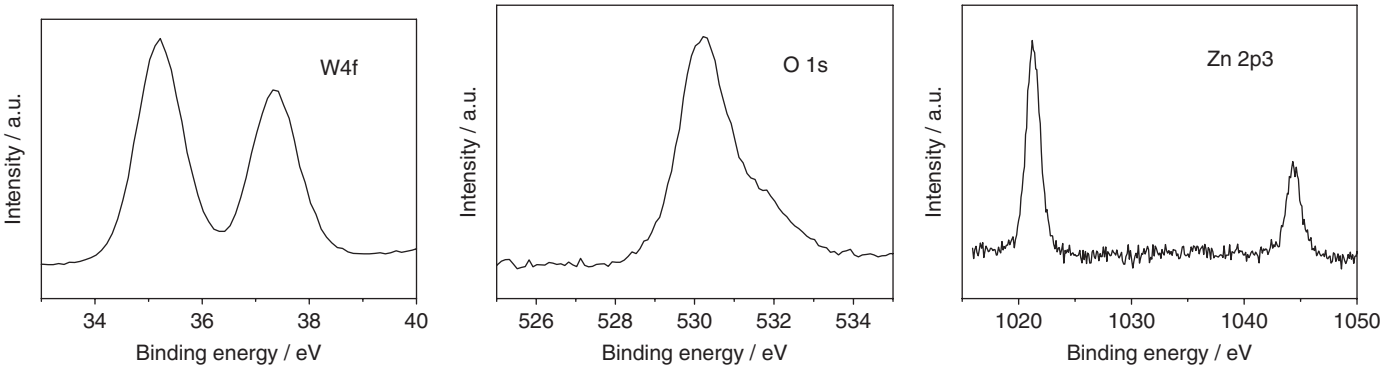

Fig. 5. X-ray photoelectron spectra of the ZnWO4 film calcined at 500 °C for 4 h.

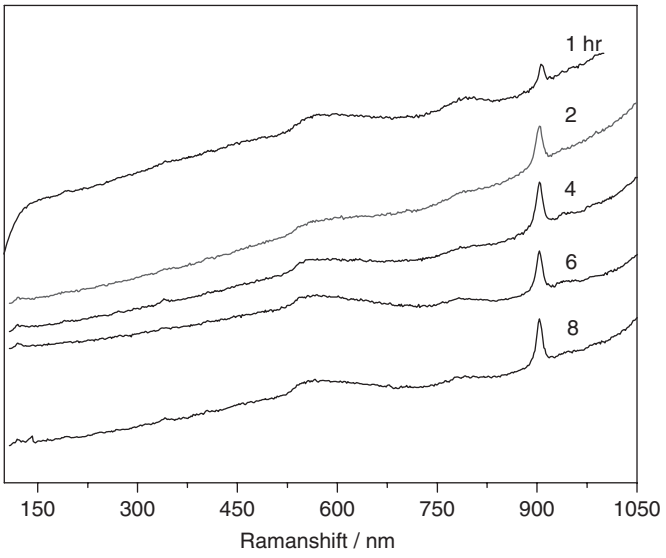

Fig. 6. Raman spectra of $ZnWO_4$-coated ITO plate with various treated time at constant temperature of 500 °C.

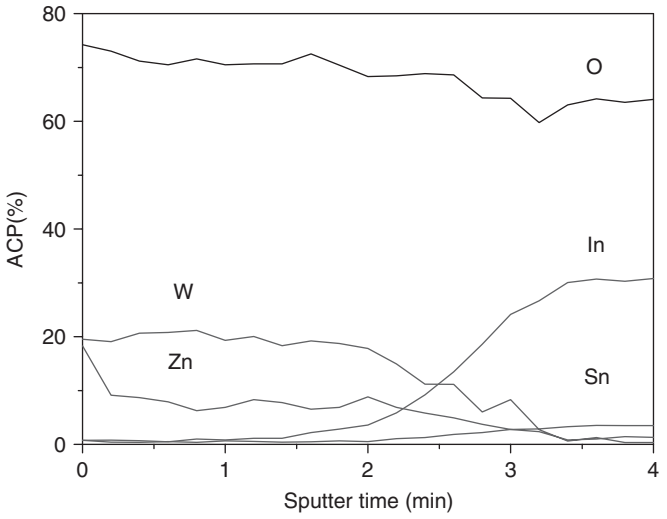

Fig. 7. Depth profile of $ZnWO_4$ film samples (coating three times).

decomposition of all organic materials continued in the precursor; their combustion and crystallization of $ZnWO_4$ have been completed below 550 °C. No significant plateau, corresponding to well-defined intermediate products, appeared in the heating process.

The DTA curve shows two exothermic peaks which could be further classified into two types of physical meaning: (1) left exothermic peak at 157 °C corresponds to initial decomposition of the precursor and (2) right exothermic peaks at 486 °C correspond to the formation of the nucleus of the crystal of $ZnWO_4$. Below 486 °C, the

resultant powders were dark brown, hard and porous, denoting an amorphous phase. It is attributed to contain a lot of carbons and ignitable organics. At the temperature of 486 °C, crystal nuclear begins to form, and the primary crystallizing process has been completed accompanying the combustion of the residual carbons and ignitable organics.

The FTIR spectra of the precursor film treated at various temperatures were presented in Fig. 9. For the precursor film, the bands at 3450 cm^{-1} (O–H stretching modes in crystallization water), 2959 cm^{-1} (C–H stretching modes), 1735 and 1378 cm^{-1} (carboxyl group stretching modes) and 1640 cm^{-1} (O–H stretching modes in alcohol), 1277 cm^{-1} (C = O stretching modes) and the weak absorption bands near 877 cm^{-1} (W–O–Zn stretching mode) seem to define the relatively dehydrated (Zn–W)–citrate polymeric complex. For the film samples treated at 450 °C, a decrease of the band at 1735 cm^{-1} produced, while the bands at 1277 and 2959 cm^{-1} disappears. For the film treated at 500 °C, the bands of the carbonyl group and carboxyl groups disappear, while new absorption bands appear between 400 and 900 cm^{-1}. The bending and stretching vibrations of Zn–O (473 and 532 cm^{-1}), W–O (633 and 710 cm^{-1}) and Zn–O–W bond (834 and 877 cm^{-1}) could be identified to the synthesized $ZnWO_4$, which is supported by the results of Raman and TG-DTA analysis. In summary, the formation process of the $ZnWO_4$ films includes three stages of the decomposition of the organic components, the formation of the amorphous $ZnWO_4$ phase, and the formation of the crystalline $ZnWO_4$ phase.

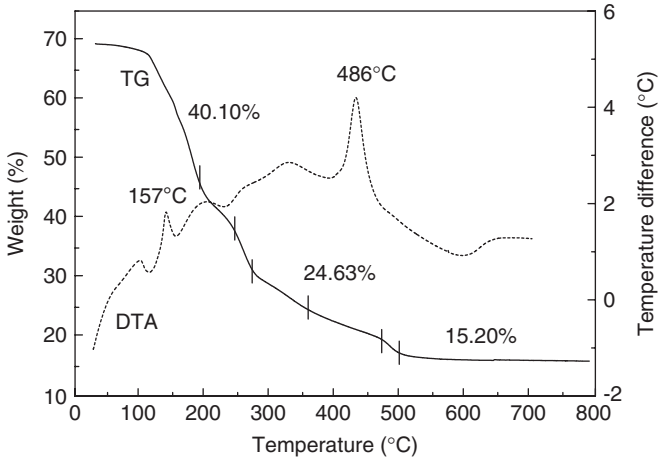

Fig. 8. TG-DTA curves of the precursor powder.

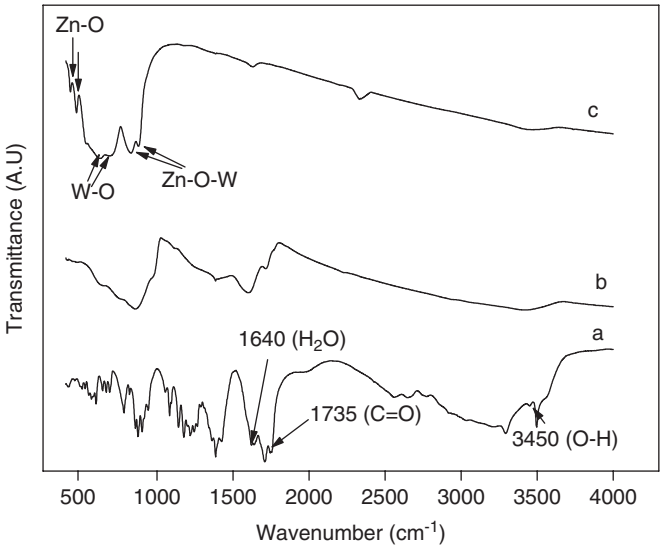

Fig. 9. FT-IR spectra of the (a) precursor and powders heat-treated at (b) 450 °C and (c) 500 °C for 4 h.

3.3. Photoelectrochemical properties of the porous $ZnWO_4$ film

3.3.1. Optical properties

Fig. 10 shows a diffuse reflection spectrum of $ZnWO_4$ film deposited onto quartz glass treated at 500 °C for 4 h as well as the powder sample. Steep shape of the spectra indicated that the UV light absorption was due to the band-gap transition instead of the transition from the impurity level. For a crystalline semiconductor, the optical absorption near the band edge follows the equation: $ahv = A(hv-E_g)^{1/n}$, where a, v, E_g, and A are absorption coefficient, light frequency, band gap, and a constant, respectively [22]. For the $ZnWO_4$, n is determined to be 2. Thus, the band gaps of the $ZnWO_4$ film were roughly estimated to be 4.01 eV as shown in the inset of Fig. 10.

Bonanni et al. [17] reported that the band gap of $ZnWO_4$ was 3.75 eV, which is lower than our experimental value. In comparison with the powder samples with grain size of ca. 50 nm prepared under same condition, the obvious blue shift can be seen. Because the crystallite size of $ZnWO_4$ for the powder and film samples is far larger than 5 nm. Therefore, the blue shift cannot result from quantum size effect. The crystallization degree may contribute to the blue shift.

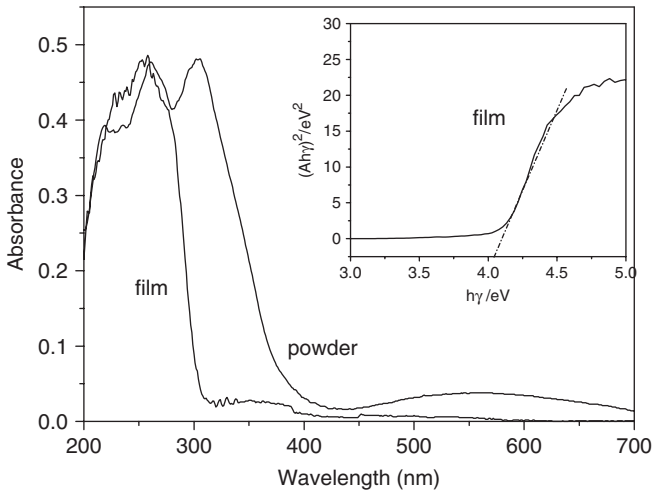

Fig. 10. DRS of $ZnWO_4$ film coated quartz substrate (25 nm) calcined at 500 °C for 4 h and the powder sample.

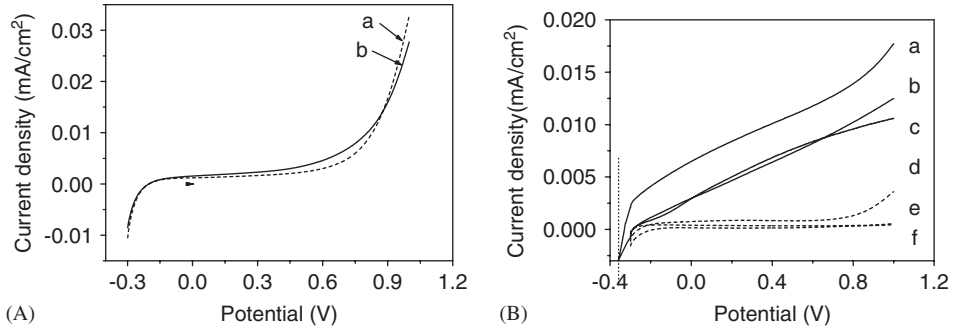

Fig. 11. Current vs. potential curves for $ZnWO_4$ film treated at various temperatures ((a) dark 450 °C; and (b) photo 450 °C) in (A) and ((a) photo 500 °C; (b) photo 550 °C; (c) photo TiO_2; (d) dark 500 °C; (e) dark 550 °C; (f) dark TiO_2) in (B) in 0.5 M Na_2SO_4 solution pH 6.0, scan rate = 10 mV s^{-1}.

3.3.2. Photocurrent response

Fig. 11(A) displayed current–voltage plots for the precursor film annealed at 450 °C under the condition of dark and UV light irradiation, respectively. The slight increase of the photocurrent may be ascribed to the photocurrent generation from the ITO substrate and/or small dielectric constant [23]. In Fig. 11(B), there was a significant photocurrent generation for the film sample treated at 500 °C. A slight decrease in photocurrent for the film samples annealed at 550 °C was also observed. The photocurrent–voltage plot of anatase film was also showed in Fig. 11(B). It was prepared from sol–gel precursor via dip-coating method and treated at 500 °C for 4 h according to previous work [24]. In comparison with the anatase film, it can be seen that the $ZnWO_4$ films generate similar, even high photocurrent at the same potential under UV light irradiation. The porous structure of the $ZnWO_4$ film offers more active sites to adsorb water and hydroxyl groups, which captured holes generated by illumination and produce active hydroxyl radicals. The porous structures also offer an advantage that the diffusion length of valence band (VB) holes formed by the band gap photo-excitation is short, because the H_2O molecules can penetrate into the pores in the whole film. These factors contribute to the high photocurrent response of the porous $ZnWO_4$ film.

Inspection of the SEM of the above films in Fig. 1 might suggest marked differences observed in their porosity as a possible reason for the varying photocurrent for film samples treated at 500 and 550 °C. It is well established that the internal surface area of dye-sensitized semiconductor electrodes affects critically their conversion efficiency. However, in the present case, despite the apparently porous structure of the sample annealed at 550 °C, its photocurrent remained relatively low in comparison with the film samples annealed at 500 °C for 4 h. Thus, the porosity does not appear as the dominant factor. The relatively large size of the particles and the nature of the interparticle contacts can be expected to explain the decreased photocurrent according to the conclusion obtained by Wahl and Augustynski [25].

3.3.3. Band structure

It is clear that the formation of $ZnWO_4$ film contribute to the apparent photocurrent. In the dark, the cathodic current is seen as a result of accumulation of electrons in $ZnWO_4$ film; in the anodic region, the anodic dark current is extremely small because no holes are available. Under UV light illumination, the photocurrent increases with the anodic potential as is commonly observed in n-type semiconductor. For the film calcined at 500 °C, the curve of the dark current density intersects with that of the photocurrent density at $V = -0.36$ V as shown in Fig. 11(B). It is known that the contact between ITO conductive electrode and the oxide semiconductor film is generally ohmic. Thus, the flat-band potential of the $ZnWO_4$ film can be roughly thought as –0.36 eV vs. SCE according to the protocol given by Bard [26]. The potential at the bottom of most n-type oxide semiconductors is about 0.10–0.30 eV more negative than the Fermi level [27]. Here, the difference for the $ZnWO_4$ film is estimated to be −0.20 eV. So, it is reasonably suggested that the top of VB was −0.56 eV.The band gap of 4.01 eV means that the potential at the bottom of the conduction band should be around 3.45 eV.

3.4. Photocatalytic activities towards degradation of RhB

The porous $ZnWO_4$ film electrode treated at 500 °C for 4 h was used to photocatalytically degrade RhB. In comparison, the degradation experiment was also carried out over the anatase film electrode. As shown in Fig. 12, the direct photolysis of RhB was present. In the presence of the porous $ZnWO_4$ film (75 nm), no noticeable variation of RhB relative concentration against time (until 8 h) without light irradiation was observed. Thus, the influence of RhB adsorption on the photodegradation could be neglected. The porous $ZnWO_4$ film electrode deposited with one time showed comparable photocatalytic activities with the anatase film electrode. The photocatalytic activity of porous $ZnWO_4$ film (75 nm) is higher than that of the anatase film with a thickness of about 85 nm. In 4 h, 62% of RhB was degraded over the porous $ZnWO_4$ film electrode, while about 51% of RhB was degraded over

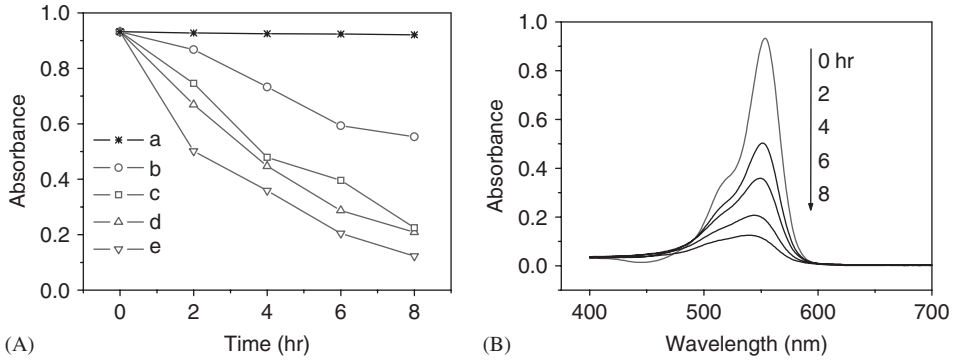

Fig. 12. (A) Variation of RhB relative concentration with irradiation time (control ((a) no light, $ZnWO_4$ film (75 nm); (b) direct photolysis; (c) photocatalytic degradation ($ZnWO_4$ film (25 nm); (d) anatase film (85 nm); (e) $ZnWO_4$ film (75 nm)). (B) UV absorbance of RhB (5 mg/L) in the photocatalytic degradation against irradiation time ($ZnWO_4$ film, 75 nm).

the anatase film electrode. At the same time, a slight shift of its maximum adsorption peak from 550 to 540 nm during the photodegradation was found (Fig. 12(B)).

It is well established that the photocatalytic activity of semiconductor is closely related to its band structure. An active photocatalyst for the decomposition of the organic compounds must have a VB with strong oxidizing ability and photogenerated holes with high mobility. Upon UV light excitation, the electronic excitation in the lower part of the conduction band is formed due to the transitions into the tungstate W 5*d* states hybridized with O 6*p* within the oxyanionic complex. The hybridized VB of $ZnWO_4$ has shown strong oxidative ability in the work described above. Meantime, the hybridization of the W 5*d* and O 2*p* levels makes the VB largely dispersed, which favors the mobility of photoholes in the VB and is benefit to the oxidation reaction [28].

The $ZnWO_4$ film has a wider band gap than the anatase film. Its bottom of the conduction band is around 3.45 eV against 2.8 eV for the anatase film. It is accepted that wider band gap energy corresponds to a more powerful redox capability. Additionally, porous films with large surface offer many active sites to adsorb water and hydroxyl group, which capture holes generated by illumination and produce many active hydroxyl radicals. Moreover, the electrolyte solution can penetrate into the pores in the $ZnWO_4$ film. Thus, the diffusion length of VB holes formed by the band gap photo-excitation is short. All of these factors are responsible for its high photocatalytic activities.

4. Conclusions

Porous $ZnWO_4$ films can be readily prepared on the ITO glass from an amorphous heteronuclear complex with the addition of PEG via the dip-coating method. The PEG suppresses the agglomeration of the $ZnWO_4$ particles and induces the formation of pore structures during the calcinations process. The phase, thickness, and crystallinity of the films were controllable by adjusting the reaction conditions. The band gap of the $ZnWO_4$ film was estimated to be ca. 4.01 eV. The top of VB and the bottom of the conduction band was estimated to be −0.56 and 3.45 eV (vs. SCE), respectively. Under UV light irradiation, the transitions of the tungstate W 5*d* states hybridized with O 6*p* within the oxyanionic complex of WO_6 result in the production of valence electron and conduction hole, which are responsible for the photocurrent generation and photocatalytic activities. The wide band gap and porous structure of the $ZnWO_4$ film contribute to its superior photoelectrochemical response and high photocatalytic activities towards the degradation of RhB. The obtained results not only reveal the novel properties of $ZnWO_4$ but also are informational in the development of novel materials applied in photovoltaic cells and photocatalysis.

Acknowledgements

This work was partly supported by the National Nature Science Foundation (20433010, 20507011), Trans-Century Training Program Foundation for the Talents by the Ministry of Education, PRC and supported by the Excellent Young Teacher Program of MOE, PR China.

References

[1] A. Mills, S.L. Hunte, J. Photochem. Photobiol. A 108 (1997) 1.
[2] M. Grazel, Nature 414 (2001) 338.
[3] M.R. Hoffmann, S.T. Martin, W. Choi, D.W. Bahnemannt, Chem. Rev. 95 (1995) 69.
[4] K. Sayama, H. Arakawa, J. Photochem. Photobiol. A 77 (1994) 243.
[5] A. Kudo, K. Omori, H. Kato, J. Am. Chem. Soc. 121 (1999) 11459.
[6] H. Kato, K. Asakura, A. Kudo, J. Am. Chem. Soc. 125 (2003) 3082.
[7] Z.G. Zou, J.H. Ye, K. Sayama, H. Arakawa, Nature 414 (2001) 625.
[8] A. Kudo, S. Hijii, Chem. Lett. (1999) 1103.
[9] J.W. Tang, Z.G. Zou, J.H. Ye, Catal. Lett. 92 (2004) 53–56.
[10] J.W. Tang, Z.G. Zou, J.H. Ye, J. Phys. Chem. B 107 (2003) 14265.
[11] S.H. Yu, B. Liu, B.M.S. Mo, J.H. Huang, X.M. Liu, Y.T. Qian, Adv. Funct. Mater. 13 (2003) 639.
[12] Z.D. Lou, J.H. Hao, M. Cocivera, J. Lumin. 99 (2002) 349.
[13] L.G. Van Uitert, S. Preziosi, J. Appl. Phys. 33 (1962) 2908.
[14] T.O. Takagi, T. Fukuzawa, Appl. Phys. Lett. 36 (1980) 278.
[15] I. Foeldvari, A. Peter, S. Keszthelyi-landori, R. Capelletti, L. Cravero, F. Schmidt, J. Cryst. Growth 79 (1986) 714.
[16] C. Santato, M. Odziemkowski, M. Ulmann, J. Augustynski, J. Am. Chem. Soc. 103 (2001) 10639.

[17] M. Bonanni, L. Spanhel, M. Lerch, E. Fuglein, G. Muller, Chem. Mater. 10 (1998) 304.
[18] Y.X. Zhang, Y.F. Zhu, R.Q. Tan, W.Q. Yao, L.L. Cao, Thin Solid Films 388 (2001) 160.
[19] H. Wullens, D. Leroy, M. Devillers, Int. J. Inorg. Mater. 3 (2001) 309.
[20] Y.F. Zhu, R.Q. Tan, J. Feng, S.S. Ji, L.L. Cao, Appl. Catal. A: Gen. 209 (2001) 71.
[21] S. Jing, L. Wei, Y.F. Zhu, J. Mol. Catal. A: Chem. 202 (2003) 187.
[22] M.A. Butler, Appl. Phys. 48 (1977) 1914.
[23] N. Sakai, Y. Ebina, K. Takada, T. Sasaki, J. Am. Chem. Soc. 126 (2004) 5851.
[24] J. Shang, W. Li, Y.F. Zhu, J. Mol. Catal. A: Chem. 202 (2003) 187.
[25] A. Wahl, J. Augustynski, J. Phys. Chem. B 102 (1998) 7820.
[26] A.J. Bard, J. Phys. Chem. 86 (1982) 172.
[27] Y. Matsumoto, J. Solid State Chem. 126 (1996) 227.
[28] M. Oshikiri, M. Boero, J.H. Ye, Z.G. Zou, G. Kido, J. Chem. Phys. 117 (2002) 7313.